SCIENCE CHINA
Chemistry

• ARTICLES •

Synchronously modulating the strength of chemical and electric field-induced passivation for robust and efficient perovskite photovoltaics

Changtan Qu[1#], Hok-Leung Loi[3,4#], Xiang Feng[1], Miao Zhang[2,4]*, Yongwen Zhang[2], Zhengyun Wang[2], Yueyue Gao[1]*, Feng Yan[3,4]*, Wai-Yeung Wong[2,4]*

[1]*Key Laboratory of Photovoltaic Materials, School of Future Technology, Henan University, Kaifeng 475004, P. R. China.*
[2]*Department of Applied Biology and Chemical Technology and Research Institute for Smart Energy, The Hong Kong Polytechnic University, Hung Hom, Kowloon, Hong Kong, P. R. China.*
[3]*Department of Applied Physics, The Hong Kong Polytechnic University, Hung Hom, Kowloon, Hong Kong, P. R. China.*
[4]*Research Centre for Organic Electronics, The Hong Kong Polytechnic University, Hung Hom, Kowloon, Hong Kong, P. R. China.*
[#] C. T. Qu and H.-L. Loi contributed equally to this work.

Received ***; accepted ***; published online ***

ABSTRACT: One of the primary challenges of perovskite solar cells (PSCs) towards commercialization is to simultaneously achieve sufficient stability and high power conversion efficiency (PCE). Here, we propose a synchronous modulation of the strength of chemical and electric field-induced passivation strategies to comprehensively heal the imperfect characteristics of perovskite. Two nitrogen-rich small molecules with asymmetric geometry, namely AS-BP and AS-AZO, were designed and synthesized. The target molecule AS-AZO featuring the most Lewis-base active sites and the largest dipole moment can effectively passivate defects of perovskite and improve built-in potential of derived PSCs. Moreover, the most flexible molecular structure of AS-AZO can ensure it as a molecular creeper towards perovskite grain, not only largely relieving the residual strain, but also reinforcing the overall passivation capability. The abovementioned effects of AS-AZO largely stabilize the perovskite and optimize the charge carrier dynamics of derived PSCs, leading to robust stability against humidity, thermal stress and light soaking along with a promising PCE of 25.12% versus that of the control one (21.82%). Our work offers valuable insights for designing molecules featuring sufficient chemical and electric field effects for synchronous passivation capability for assembling robust and efficient PSCs.

KEYWORDS: Perovskite solar cells, Asymmetrical small molecules, Stability, Chemical passivation, Electric field-induced passivation

Citation:

1 Introduction

Over the past decade, perovskite solar cells (PSCs) have aroused unprecedented attention in academic and industrial communities on account of their exceptional photovoltaic performance and cost-effective manufacturing.[1, 2] Up to now, the state-of-the-art power conversion efficiency (PCE) of the laboratory-scale single-junction PSCs has surpassed 27%, which is highly competitive compared to the market-leader crystalline silicon solar cells.[3-7] Despite attractive efficiency having been achieved for PSCs, their instability, especially that of the perovskite absorber layer under external stimuli is still a significant challenge towards commercialization.[8] Generally, the perovskite film commonly suffers from intrinsic defects, residual strain and numerous grain boundaries, largely deteriorating the efficiency as well as the stability of derived PSCs.[9, 10] In this regard, developing effective methods to simultaneously heal those imperfect characteristics of perovskite is crucial for promoting the stability and efficiency of PSCs.

Recently, adopting chemical and electric field-induced synchronous passivation towards the perovskite have shown

*Corresponding authors M. Zhang (bjtumiao.zhang@polyu.edu.hk); Y. Y. Gao (gaoyueyue@henu.edu.cn); F. Yan (apafyan@polyu.edu.hk); W.-Y. Wong (wai-yeung.wong@polyu.edu.hk)

promise for repairing their imperfect characteristics to simultaneously enhance the stability and efficiency of PSCs.[11, 12] For instance, Ma and co-workers revealed that the phenmethylammonium ions (PMA^+) applied to post-treat the perovskite film could not only insert chemical passivation toward the intrinsic defects of perovskite to weaken the non-radiative recombination, but also impart large surface dipole to improve the splitting of hole quasi-Fermi level. Eventually, the chemical and electric field-induced synchronous passivation of PMA^+ leads to an overall increase in shelf-stability as well as a higher PCE of 24.10% for target devices versus that of the control one (21.44%).[13] Very recently, Xu *et al*. applied 1-adamantanamine hydroiodide (ADAI) to construct robust chemical interactions and electric field-derived passivation towards the perovskite layer. The ADAI modified layer could inhibit charge recombination and minimize band-misalignment, resulting in an enhanced endurance against illumination and a promising PCE of 25.13% compared to the control one (22.35%).[14] It has been demonstrated that the chemical and electric field-induced synchronous passivation endowed by alkyamine-type organic molecules towards the perovskite film can simultaneously improve the stability and efficiency of PSCs to some extent. However, due to the weak chemical interactions arising from their limited functional groups of alkyamine-type organic molecules, the interface reconstruction and loss of initial properties would be triggered under heat or light, which greatly deteriorate the efficiency and long-term stability of PSCs[15, 16]. Consequently, developing molecules featuring sufficient chemical and electric field-induced synchronous passivation and providing the derived molecular design guidelines is highly important and urgent to fabricate long-term robust yet efficient PSCs.

Herein, we designed and synthesized three benzothiadiazole-based organic molecules with different substituent groups (triphenylamine/AS, bipyridine/AS-BP, (phenyldiazenyl)pyridine/AS-AZO). Then, they were incorporated into perovskite to comprehensively heal its imperfect characteristics. Among those molecules, AS-AZO exhibits the most Lewis-base active sites and the largest dipole moment, resulting in the most efficient chemical and electric filed-induced synchronous passivation. Meanwhile, the most flexible molecular structure of AS-AZO can effectively relieve the residual strain in perovskite. The overall effects of AS-AZO largely stabilize the perovskite and optimize the charge carrier dynamics of derived PSCs. Consequently, the champion PVK/AS-AZO devices deliver robust stability against humidity, thermal stress and light soaking accompanied by a promising PCE of 25.12%. More importantly, the champion PVK/AS-AZO devices preserve 93.2% of its initial efficiency after continuous operation for 600 h, being superior to the control one.

2 Results and discussion

The synthetic routes of the triphenylamine-based organic molecules (**Figure 1**a) involved in this work are illustrated in **Scheme S**1. Their molecular structures are characterized by Proton Nuclear Magnetic Resonance Spectroscopy (^{1}H-NMR) and Single Crystal X-ray Diffraction (Figure S1-S3). The single crystal structure of AS-BP was successfully obtained with the CCDC number of 2441617. All three molecules display decomposition temperature (5% weight loss) over 280 ºC (Figure S4), demonstrating their good thermal stability for the fabrication and operation of PSCs. Furthermore, the AS-AZO films also exhibit excellent stability at a long-time heating condition (Figure S5). After heating at 65 °C for 5 hours, the long wavelength absorption peaks induced by the intramolecular charge transfer (ICT) remain unchanged, while the peaks are gradually blue shift and the intensity is gradually decreased for the AS and AS-BP films. The conductivity of devices with the structure of ITO/AZO/Ag is more stable that of AS and AS-BP-based devices after 5-hour heating, demonstrating that AS-AZO features superior chemical and electrical stability compared to both AS and AS-BP. Three materials exhibit good solubility in common organic solvents such as DMSO, DMF, chlorobenzene (CB), etc, which is beneficial for solution-processed engineering. The intramolecular charge transfer absorption peak of AS-AZO in film state versus that in solution shifts towards the longer wavelength by 36 nm (Figure S6) as compared to AS (26 nm) and AS-BP (33 nm), indicating the stronger intermolecular interaction arising from more non-covalent interaction in the former.[17] The non-covalent interaction-rich feature of AS-AZO is attributed to their more Lewis-base active sites, which are favorable for constructing multiple interactions with the organic cations, halide anions and under-coordinative Pb^{2+} ions in perovskite to comprehensively enhance its stability.[18]

The density functional theory (DFT) calculations at B3LYP/6-31G* level were first applied to investigate the theoretical properties of AS-type molecules. As shown in **Figure 1**b, the dihedral angles between the terminal groups and the adjacent units are 10.7º/11.0º, 10.2º/8.5º and 120.4º/102.6º for AS, AS-BP and AS-AZO, respectively. The tortile molecular structure of AS-AZO as confirmed by its side-view geometry (Figure S7a) could further render it as a molecular creeper to provide reliable yet compact contact with the perovskite grain to obtain better defect passivation and moisture resistance. Compared to AS, the electron density at the HOMO/LUMO energy level of AS-BP and AS-AZO is inhomogeneously distributed over their molecular backbone (Figure S7b-c), implying their strong intramolecular charge transfer capability, which can assist the charge transfer in perovskite/AS-BP or perovskite/AS-AZO mixtures. As displayed in **Figure 1**c, AS-AZO presents the most asymmetrical molecular structure and electron-rich characteristics locating its end-groups, resulting in the largest dipole moment of 4.92

Debye among the three synthesized molecules. Moreover, the end groups of AS-AZO would tend to point towards the perovskite and the triphenylamine unit would point away from the perovskite, which results in the increased interfacial dipole strength of AS-AZO towards the perovskite and thus sufficient electric field-induced passivation. Therefore, the largest dipole moment as well as the most electron-rich characteristics of AS-AZO are beneficial for imparting strong chemical and electric field-induced passivation towards the perovskite, which are anticipated to improve the built-in potential as well as *Voc* of the derived PSCs.[19, 20]

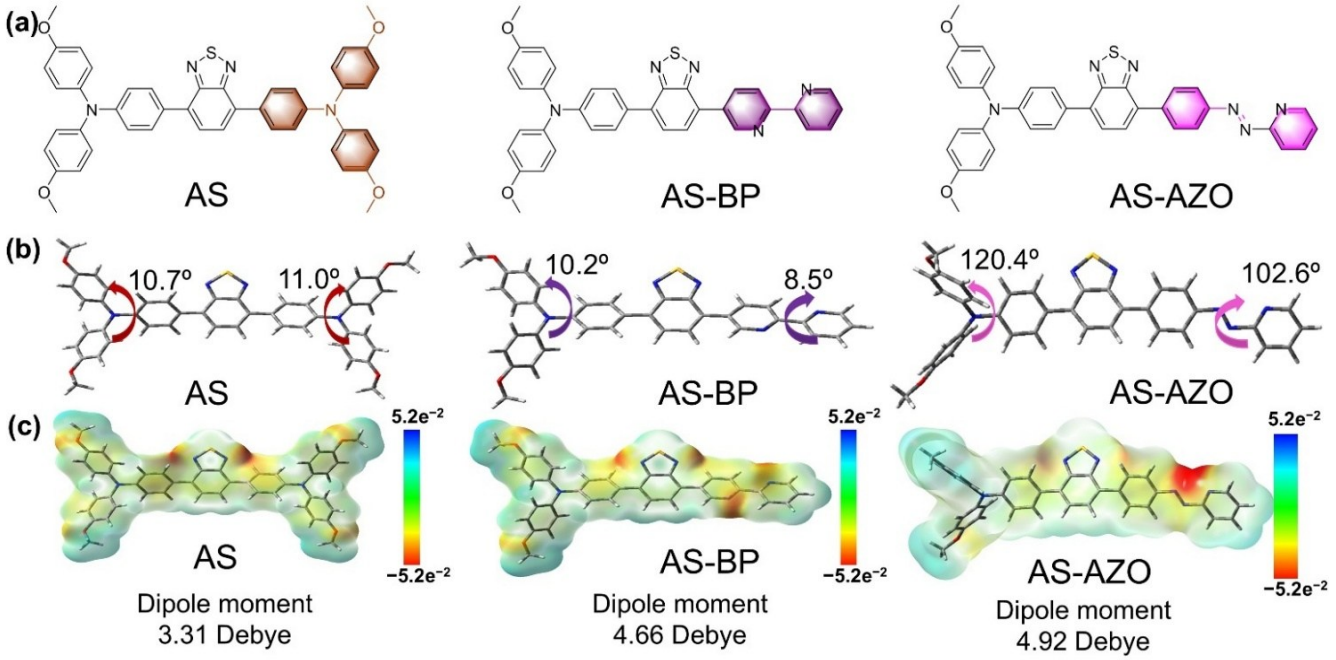

Figure 1. (a) Molecular structures of AS-type molecules. (b) Molecular geometry of AS-type molecules from top view. (c) Electrostatic surface potential and dipole moment of AS-type molecules.

Encouraged by the superior theoretical properties of AS-AZO, the DFT calculations based on the CP2K package with Perdew-Burke-Ernzerhof function were further implemented to study the interactions between AS-type molecules and perovskite.[21] It is noted that the adsorption energies of AS, AS-BP and AS-AZO towards perovskite are −0.49 eV, −0.66 eV and −1.56 eV, respectively (Figure S8). Meanwhile, AS-AZO displays more distinct electron transport towards perovskite in comparison with AS and AS-BP (**Figure 2**a). The DFT result reveals that AS-AZO features stronger interaction with perovskite versus AS and AS-BP. The stronger interaction between AS-AZO and perovskite could be visually corroborated by the number of remaining molecules after the perovskite/AS-type film being washed with CB (**Figure 2**b and Table S1). After washing, the residual content of the AS-AZO molecules was significantly higher than those of AS and AS-BP molecules as confirmed by the higher percentage of S by weight in the EDS mapping (AS: 1.35%; AS-BP: 2.82%; AS-AZO: 4.19%). Moreover, the weight ratio of Pb to S for PVK/AS and PVK/AS-BP films is markedly increased from 14:4 and 15:3 to 20:1 and 25:2, respectively. For PVK/AS-AZO sample, the ratios before and after washing show no much difference (from 13:4 to 15:5), which is attributed to the strong interaction between AS-AZO and perovskite. Besides, the N-H stretching vibration peaks of FAI observed at 3362 cm^{-1} and 3174 cm^{-1} would gradually shift towards smaller wavenumbers after being mixed with AS-type molecules, which follows the trend of AS<AS-BP<AS-AZO (**Figure 2**c and Figure S10), implying the presence of stronger hydrogen bond in FAI/AS-AZO mixture. The N-H stretching vibrational peak exhibits the same trend for perovskite/AS-type molecules samples, indicating that AS-AZO exhibits stronger hydrogen bonding interactions with perovskite (Figure S12).[22] This finding is further corroborated by the DFT calculations and the ^{1}H-NMR spectra of FAI/AS-type samples (Figure S9 and Figure S11). The adsorption energy reaches -5.43 eV between AS-AZO and FA^{+}, and the largest chemical shift was observed for FAI/AS-AZO sample. As exhibited in **Figure 2**d and Figure S13a, the core XPS spectra of Pb in the perovskite film present distinct doublet peaks at 137.1 eV and 142.0 eV, which are indexed to the binding energy of the Pb $4f_{7/2}$ and Pb $4f_{5/2}$, respectively.[23] Besides, the perovskite film displays two additional XPS peaks of Pb at 135.3 eV and 140.3 eV, being attributed to the metallic Pb, which is capable of aggravating the charge recombination and accelerating the decomposition of perov-

skite.[24] Comparatively, the XPS spectra of Pb in perovskite/AS-type film gradually shift towards the lower binding energy accompanied with the reduction of the Pb^{2+} concentration in the order of AS<AS-BP<AS-AZO (Figure S13b). The result demonstrates the most effective passivation by AS-AZO towards perovskite, which is corroborated by the corresponding lower Urbach energy of PVK/AS-AZO film than PVK film (Figure S14).[25] Furthermore, the XPS spectra of I in perovskite/AS-type film (Figure S13c), the FTIR spectra of PbI_2/AS-type film (Figure S15) and the ^{1}H-NMR spectra of PbI_2/AS-type mixture (Figure S16) comprehensively confirm the presence of stronger interaction of AS-AZO with Pb^{2+} cations and I^- anions in perovskite. The abovementioned result reveals that AS-AZO can endow more interaction active sites with all perovskite composition than AS and AS-BP (**Figure 2**e), largely improving the stability and efficiency of the former PSCs.

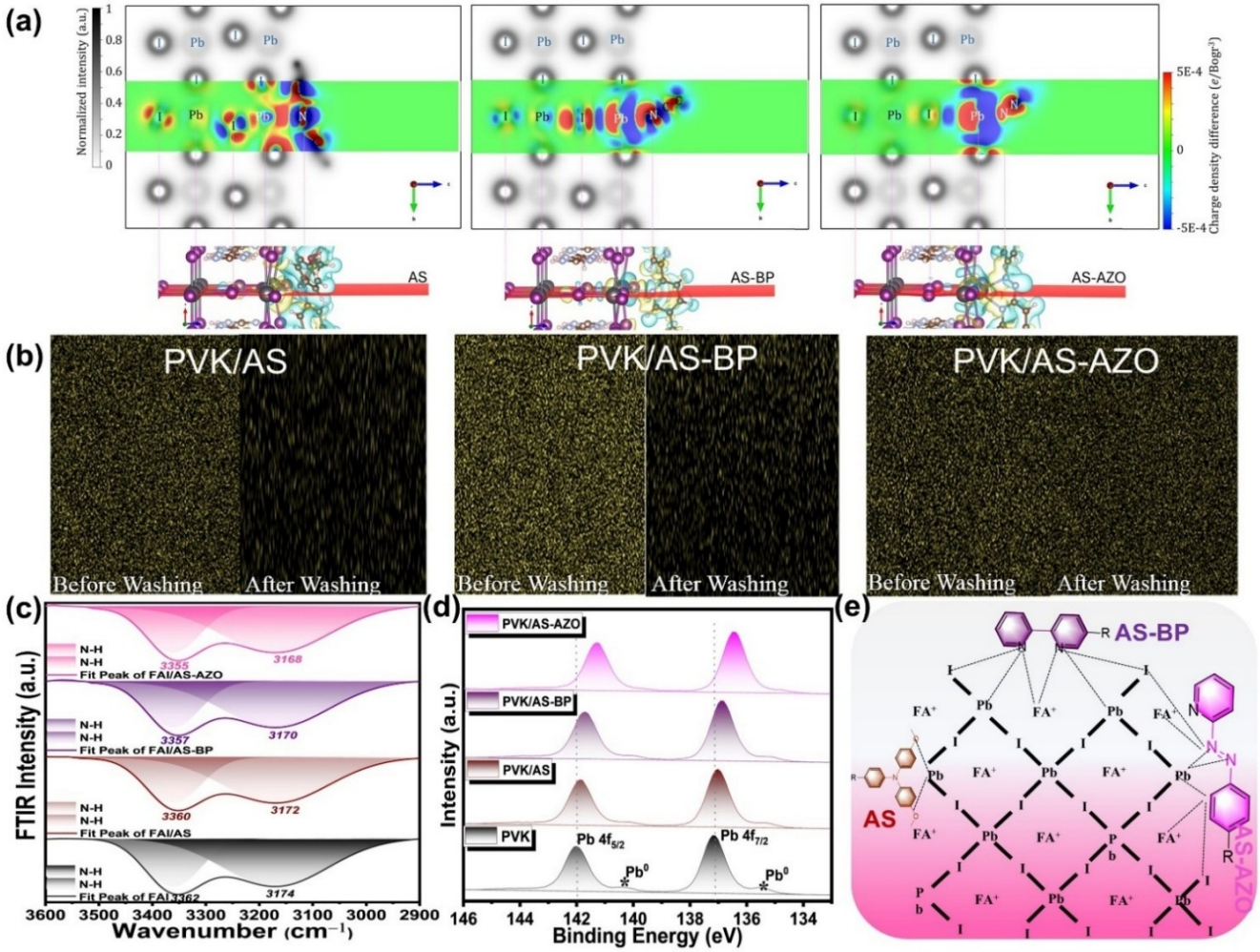

Figure 2. (a) Differential charge density of AS-type molecules adsorbed upon $FAPbI_3$, where the yellow/blue areas represent the electron-accepting/donating unit. (b) The sulfur EDS mapping in perovskite/AS-type film being washed with CB or not. (c) FTIR spectra of FAI and FAI/AS-type power. (d) XPS spectra of Pb element of $FAPbI_3$ and $FAPbI_3$/AS-type film. (e) The interaction scheme between AS-type molecules and $FAPbI_3$.

It is worth noting that the soft characterisitics of AS-AZO as well as the stronger interaction with perovskite can feature great potential to relieve the residual strain in the perovskite film.[26] Therefore, the depth-dependent grazing incident X-ray diffraction (GIXRD) in 2θ–sin^{2}ψ mode was used to evaluate the evolution of residual strain across perovskite film. Generally, the slope of 2θ–sin^{2}ψ linear function could be deduced from the equation:

$$\sigma = -\frac{E}{2(1+\upsilon)}\frac{\pi}{180^o}cot\theta_0\frac{\partial(2\theta)}{\partial(sin^2\psi)} \quad (1)$$

where E, υ and σ represent the perovskite modulus (10 GPa), the poisson's ratio of perovskite (0.3) and the strain stress of perovskite, respectively.[27, 28] As shown in **Figure 3**a, there is a pronounced shift of (100) diffraction peak of PVK to larger 2θ when the incident angle ψ varies from 10° to 50°, suggesting the reduction of (100) crystal plane distance and the presence of severe tensile strain (K_{slope} = −0.0083 and σ = −101.7 MPa, **Figure 3**b-d).[29] The severe tensile strain can accelerate ion migration and induce serious non-radiative recombination, being detrimental for the efficiency and long-term stability of PSCs.[30] In contrast, the modified PVK

film displays reduced 2θ shifts of (100) diffraction peak across different ψ angles, implying the gradually inhibited tensile strain for PVK/AS film (K_{slope} = −0.0053 and σ = −65.7 MPa) and PVK/AS-BP film (K_{slope} = −0.0037 and σ = −45.5 MPa). Moreover, the (100) diffraction peak of PVK/AS-AZO shows almost negligible shifts, indicating effective diminishing of the tensile strain (K_{slope} = −0.0012 and σ = −15.2 MPa). The above phenomenon should be ascribed to the stronger interaction between AS-AZO and perovskite due to the more Lewis-base active sites as well as softer molecular structure of AS-AZO than its counterparts. The tensile strain relief of PVK/AS-AZO would provide additional assistance for assembling operation-robust and efficient PSCs.

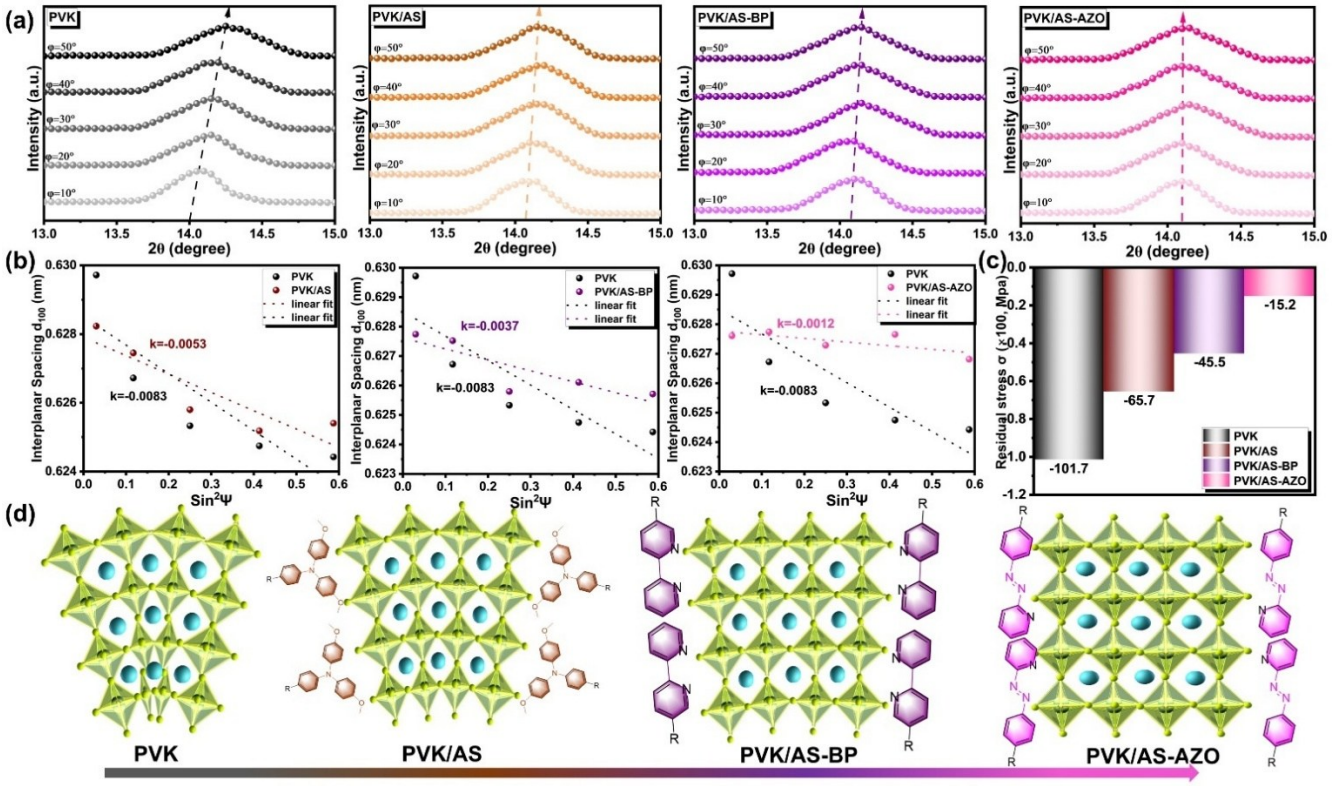

Figure 3. (a) GIXRD spectra of PVK ($FAPbI_3$) and PVK/AS-type films. (b) Linear relationship obtained from 2θ of (100) crystal plane with different incidence angle. (c) Calculated residual strain of perovskite film. (d) The schematic representation of the strain state of perovskite film.

Besides the defect passivation and residual strain relief of AS-type molecules towards perovskite, their effects on the crystalline quality and the charge carrier dynamics of perovskite were then investigated. As depicted in **Figure 4**a, the pure PVK film exhibits irregular yet small grains distribution (average grain size (S_{av}) of 0.67 nm, Figure S17), multi-stacked crystalline grains along the vertical direction and rough surface with the root-mean-square roughness (RMS = 34.1 nm, **Figure 2**e). Comparatively, the uniform, compact and large grains distribution (S_{av} of 0.88 nm and 0.94 m, **Figure 4**b-c and Figure S17) as well as smooth surface with RMS of 29.3 nm and 20.4 nm (**Figure 4**f-g) could be observed for PVK/AS and PVK/AS-BP film, respectively. Besides, the fewer transverse grain boundaries along the vertical direction are noticed for PVK/AS and PVK/AS-BP film. In contrast, PVK/AS-AZO film displays the most compact, the largest grains distribution (S_{av} of 1.12 nm, **Figure 4**d and Figure S17) as well as the smoothest surface with RMS of 18.5 nm (**Figure 4**h). Meanwhile, PVK/AS-AZO film depicts monolithic yet single-crystalline-line grains along the vertical direction (**Figure 4**d) as well as the preferential crystalline orientation along the (100) crystalline plane (Figure S18). The structural perfections of PVK/AS-AZO film are highly beneficial for the longitudinal charge transfer, charge recombination suppression and photon harvesting (Figure S19), being conducive to improving the efficiency of derived PSCs.[31, 32]

Additionally, the ultraviolet photoelectron spectroscopy (UPS) was performed to delve into the electronic energy levels of perovskite films. As shown in **Figure 4**i and Figure S20a, the conductive band minimum (E_c) and valance band maximum (E_v) of PVK film are located at −5.77 eV and −4.24 eV, respectively. Comparatively, the electronic energy level of modified PVK films is gradually up-shifted, which should be originated from the dipole moment effect of AS-type molecules.[33, 34] The energy-offset (E_{off}) between the E_v of modified PVK film and the HOMO energy level of Spiro-mF is successively decreased to 0.26 eV, 0.24 eV and 0.21 ev for PVK/AS, PVK/AS-BP and PVK/AS-AZO film,

respectively, versus that of the pure PVK film (0.58 eV). Further analysis via KPFM (Figure S20b) reveals that the contact potential difference for AS-AZO is relatively large (0.53 V), exceeding that of PVK, AS, and AS-BP (0.41 V, 0.46 V, and 0.50 V, respectively). The electronic energy levels of the modified PVK film exhibit a progressive upward shift, which is attributed to the dipole moment effect of AS-type molecules (Figure S20c). The reduced E_{off} is favorable for improving the hole transfer efficiency, which is confirmed by the derived enhanced steady-state PL quenching efficiency (**Figure 4**j and Table S2) and the corresponding shortened charge carrier lifetime (**Figure 4**k and Table S3).

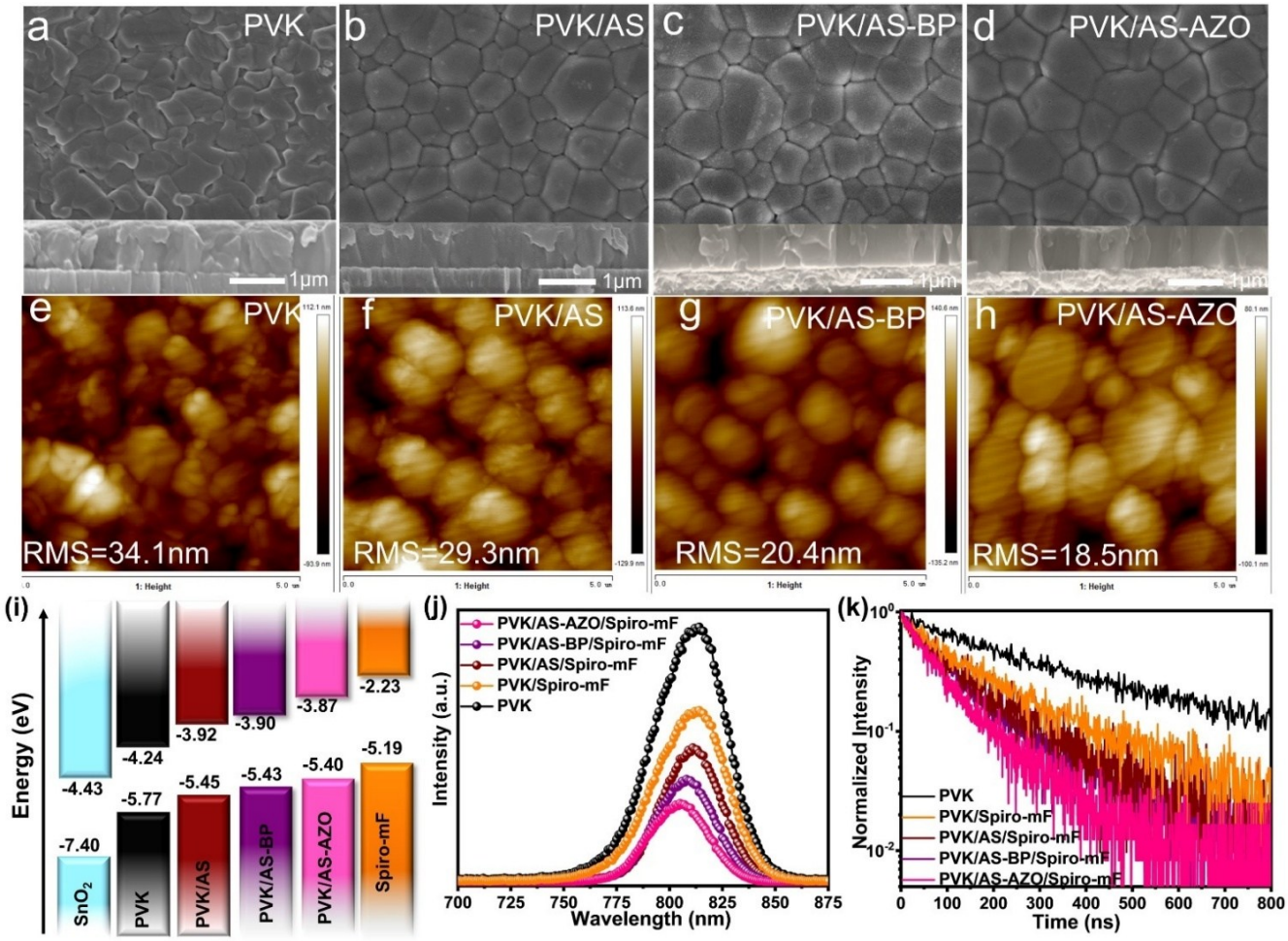

Figure 4. (a-d) The top view and cross-section view of perovskite films deposited upon ITO/SnO_2 substrates. (e-h) AFM images of perovskite films deposited upon ITO/SnO_2 substrates. (i) Energy level diagram of main components in PSCs. (j) Steady state PL spectra and (k) TRPL spectra of perovskite films with spiro-mF HTL.

Inspired by the most sufficient chemical and electric field-induced synchronous passivation towards perovskite given by AS-AZO, the PSCs with device architecture of ITO/SnO_2/PVK/Spiro-mF/Au (**Figure 5**a) were fabricated to investigate its effect on the photovoltaic efficiency. It is noted that Spiro-mF rather than Spiro-OMeTAD selected for the hole transporting layer is attributed to its higher glass transition temperature, deeper HOMO energy level and stronger hydrophobicity, hence benefiting for constructing efficient moisture/thermal-resistance PSCs.[35] The current density-voltage (*J-V*) curves are displayed in **Figure 5**b and Figure S21-S24, and the detailed photovoltaic parameters of PSCs are listed in **Table 1** and Table S4-S6.

As shown in **Figure 5**b, the control devices (PVK) depict short-circuit current density (J_{sc}) of 25.01 mA/cm^2, open-circuit voltage (V_{oc}) of 1.126 V and fill factor (FF) of 77.48%, eventually leading to a modest PCE of 21.82%. Comparatively, the PCE of PVK/AS and PVK/AS-BP devices increased to 22.58% and 23.92%, respectively, along with the synchronously enhanced photovoltaic parameters. Notably, the PVK/AS-AZO devices delivered a further enhanced PCE of 25.12% accompanied with notable V_{oc} of 1.181 V and FF of 82.92%. The gradually increased PCE along with the enhanced V_{oc} for devices (PVK<PVK/AS<PVK/AS-BP<PVK/AS-AZO) reveals the efficacy of the chemical and electric field-derived passivation effects through synchro-

nous regulation strategies. The synchronous enhanced passivation capability of PVK/AS-AZO devices can largely reduce the hysteresis index (HI, in the inset of **Figure 5**c) to 1.27% compared to the control device (9.90%).[36] As shown in **Figure 5**d, the integrated current density of all devices obtained from the IPCE spectra is consistent well with the J_{sc} in the *J-V* measurement, confirming the reliability of J_{sc} in *J-V* measurement. Additionally, not only the PVK/AS, PVK/AS-BP and PVK/AS-AZO devices display higher average PCE of 21.62%, 23.27% and 24.67% than the control one (20.67%), but also their narrower PCE distribution demonstrates good reliability yet high reproducibility of modified PSCs (**Figure 5**e). Furthermore, the steady state power output (SPO) of the champion devices at the bias voltage near maximum power point (MPP) condition was recorded in **Figure 5**f. Compared to the fluctuation and the declined SPO behavior of the control device (19.99%), the SPO value of the modified one almost keeps constant yet higher value especially for the PVK/AS-AZO devices (25.05%), suggesting their improved yet stable photovoltaic performance.

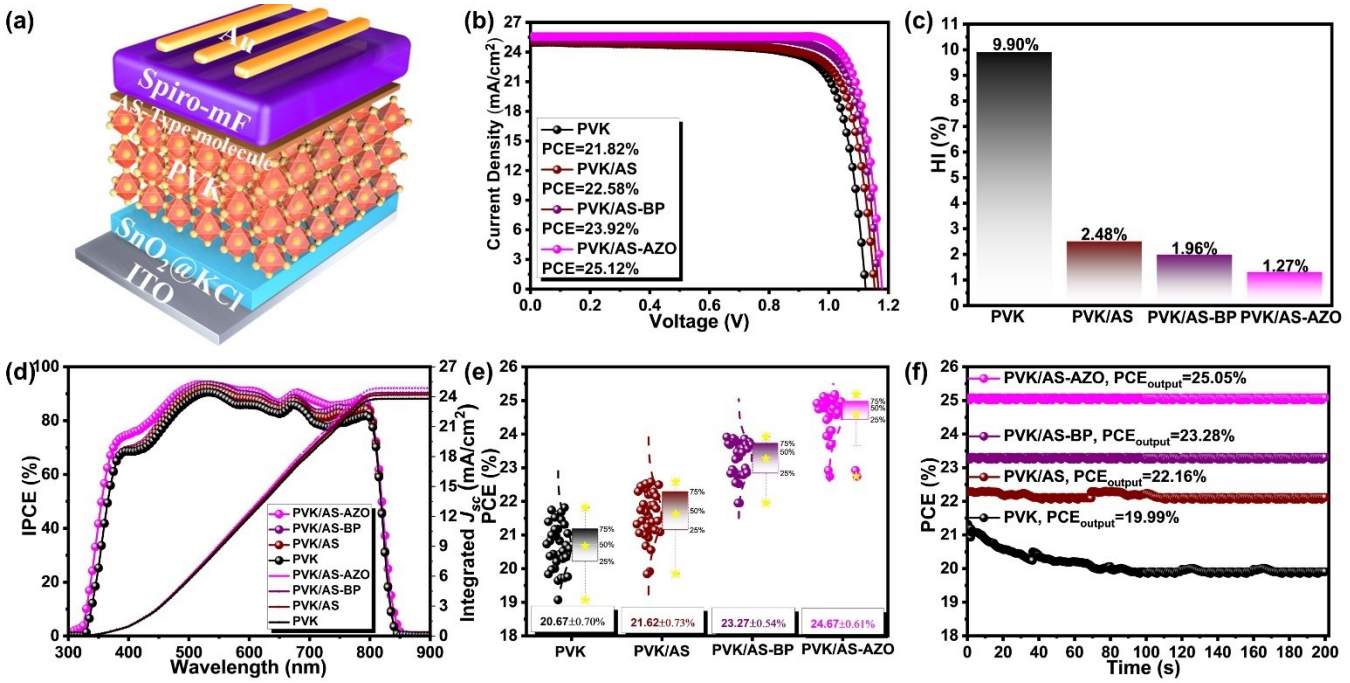

Figure 5. (a) Device structure of perovskite solar cells. (b) The *J-V* curves of champion devices measured from the reverse scan direction. (c) The hysteresis index of champion devices. (d) The IPCE spectra and integrated current density of champion devices. (e) The PCE distribution of champion devices. (f) The steady state power output of champion devices.

Table 1. Photovoltaic properties of champion devices.

Devices	Scan direction	V_{oc} (V)	J_{sc} (mA/cm^2)	*FF* (%)	PCE_{max} (%)	$PCE_{average}$ (%)
PVK	FS[a]	1.105	24.04	77.48	19.66	20.67±0.70
	RS[b]	1.126	25.01	77.48	21.82	
PVK/AS	FS	1.148	25.04	76.60	22.02	21.62±0.73
	RS	1.153	25.14	77.90	22.58	
PVK/AS-BP	FS	1.158	25.01	80.97	23.45	23.27±0.54
	RS	1.164	25.33	81.13	23.92	
PVK/AS-AZO	FS	1.179	25.33	83.04	24.80	24.67±0.61
	RS	1.181	25.65	82.92	25.12	

[a] forward scan and [b] reverse scan.

To provide an insight into the improved photovoltaic performance of the modified devices based on AS-type molecules, the systematic charge carrier dynamics of champion devices were implemented. The thermal admittance spectroscopy was first conducted to investigate the energetic distribution and quantization of the trap density of state (DOS) of champion devices. As depicted in **Figure 6**a, all modified devices present significantly diminished DOS values across the entire energy-level depth region, demonstrating the passivation of AS-type molecules towards perovskite.[37, 38] The passivation of AS-type molecules towards perovskite leads to the prolonged charge carrier lifetime of 1.86 μs, 2.17

μs and 3.23 μs for PVK/AS, PVK/AS-BP and PVK/AS-AZO devices versus that of the control one (1.41 μs, **Figure 6**b).[39-41] The abovementioned result demonstrates the inhibited charge recombination in the modified devices, being confirmed by their smaller ideality factor (*n*, Figure S25), lower leakage current density and larger rectification ratio (Figure S26).[42-44] Moreover, the space-charge-limited-current (SCLC) method was applied to quantify the defect passivation of AS-type molecules towards perovskite. In general, the trap density (N_t) can be calculated from the equation:

$$N_t = \frac{2\varepsilon_r\varepsilon_0 V_{TFL}}{eL^2} \quad (2)$$

where *e, L,* ε_r, ε_o and V_{TFL} denote element charge, thickness of perovskite film, relative dielectric constant of perovskite film (ε_r = ~34) and permittivity of free space (8.85×10^{-12} Fm^{-1}), respectively.[45-47] As shown in **Figure 6**c, compared to the V_{TFL} (1.208 V) of the control device, the corresponding values gradually decreased to 0.556 V, 0.381 V and 0.189 V for PVK/AS, PVK/AS-BP and PVK/AS-AZO devices, respectively. Naturally, the PVK/AS (1.26×10^{16} cm^{-3}), PVK/AS-BP (7.79×10^{15} cm^{-3}) and PVK/AS-AZO devices (3.38×10^{15} cm^{-3}) present lower N_t than the control one (3.07×10^{16} cm^{-3}).

In addition, transient photocurrent (TPC) measurement was implemented to study the charge carrier collection process. As exhibited in **Figure 6**d, the photocurrent decay time of the modified devices is gradually shortened to 2.15 μs, 1.08 μs and 0.87 μs for AS, AS-BP, AS-AZO modified devices, respectively, compared to the control one (2.68 μs).[48-50] The TPC result suggests the improved charge carrier collection efficiency in the modified devices, which is further verified by the photocurrent density (J_{ph}) versus effective voltage (V_{eff}) measurement in **Figure 6**e.[51-53] Furthermore, the capacitance−voltage measurement following the Mott–Schottky method was implemented (**Figure 6**f).[54-56] Generally, the relationship between capacitance (*C*) and voltage could be described by the equation:

$$\frac{1}{C^2} = \frac{2}{q\varepsilon_r\varepsilon_0 N_D}\left(V_{bi} - V - \frac{KT}{q}\right) \quad (3)$$

where *V,* V_{bi} and N_D represent applied potential, built-in potential and background majority carrier density, respectively.[57-59] As shown, the larger V_{bi} of 1.01 V, 1.07 V and 1.12V can be observed for PVK/AS, PVK/AS-BP and PVK/AS-AZO devices, respectively, in comparison with the control one (0.99 V). Notably, the larger V_{bi} is not only beneficial for facilitating charge collection, but also conducive to suppressing charge accumulation and derived recombination, being directly confirmed by the smaller slope in Mott-Schottky curves (**Figure 6**f) as well as the weaker bimolecular recombination (Figure S27) in the modified devices. The overall results comprehensively indicate that synchronously fine-tuning the strength of the chemical and electric field-induced passivation effects can optimize the charge carrier dynamics for improving the efficiency of derived PSCs.

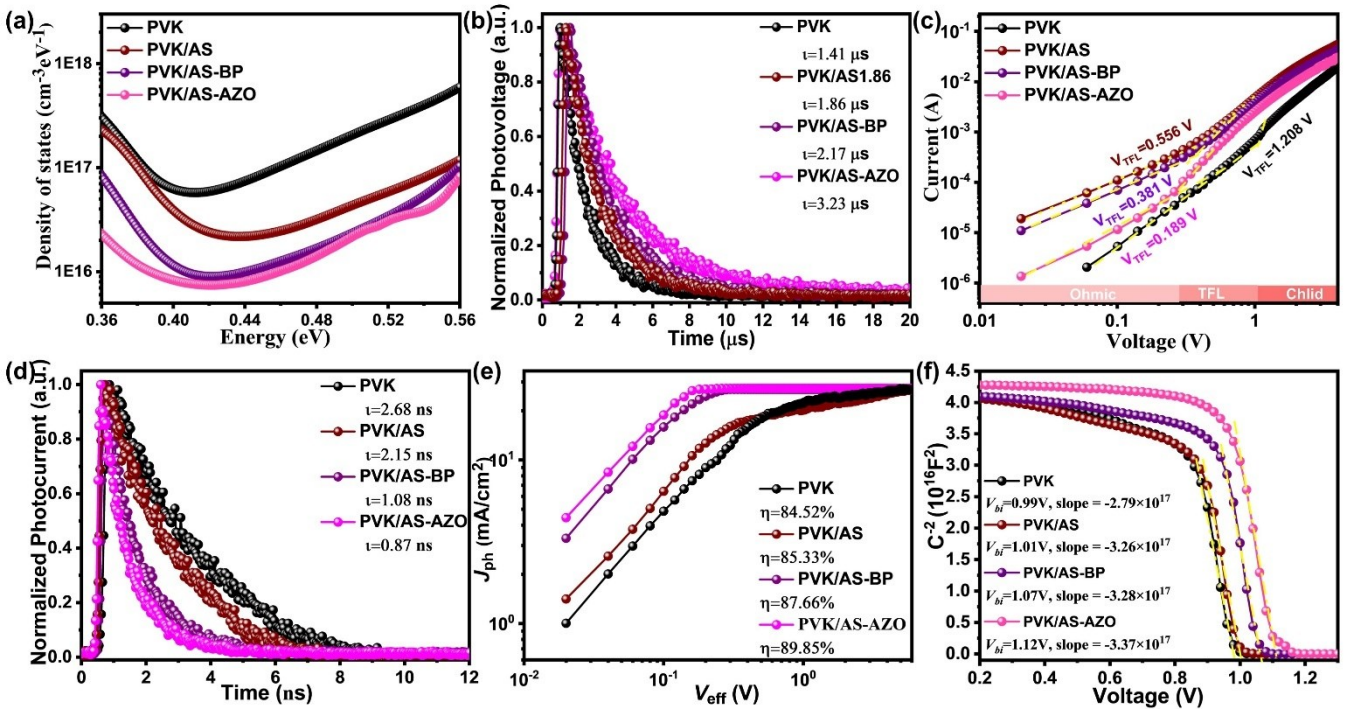

Figure 6. (a) tDOS curves of the pristine and target devices. (b) TPV spectra of the pristine and target devices. (c) SCLC characterization of hole-only devices. (d) TPC spectra of the pristine and target devices. (e) J_{ph} versus V_{eff} curves of champion devices. (f) Mott-Schottky curves of champion devices.

Relative to the efficiency, the device stability of PSCs should be the most prominent challenge needed to be addressed towards commercialization.[60-63] Therefore, the shelf storage stability of champion devices in the dark at 25 °C with relative high humidity of ~65% was firstly assessed. As shown in **Figure 7** and Table S7, the control devices are only capable of remaining 56.11% of their initial efficiency after storing 600 h. While the remaining efficiency can be increased to 62.55% and 79.87% for PVK/AS and PVK/AS-BP devices, respectively. Moreover, PVK/AS-AZO devices preserve 89.26% of their initial efficiency after being stored in the same period. The strongest endurance of PVK/AS-AZO devices against moisture is partially originated from the highest hydrophobicity of PVK/AS-AZO film (**Figure 7**b).[64] Secondly, the thermal stability of champion devices in a nitrogen glovebox at ~65°C was evaluated. As depicted in **Figure 7**c and Table S8, the control devices present poor thermal stability with 24.11% of their initial efficiency being maintained after suffering from thermal stress for 600 h. In contrast, the remaining efficiency/initial efficiency ratios are improved to 58.40%, 70.77% and 77.83% for PVK/AS, PVK/AS-BP and PVK/AS-AZO devices, respectively. We noted that the good thermal stability of PVK/AS-AZO-based devices should be partially ascribed to inherent structural stability of AS-AZO. Finally, the operational stability of champion devices using the maximum power point (MPP) tracking under 1 sun white LED array in a nitrogen glovebox was investigated. As exhibited in **Figure 7**d and Table S9, compared to the rapidly declined behavior of the efficiency for the control device, the decaying rate of the modified devices is largely suppressed especially for PVK/AS-BP and PVK/AS-AZO based devices. It's noted that PVK/AS-BP and PVK/AS-AZO based devices still preserve over 91% of their initial efficiency after MPP tracking for 600 h, being superior to the control device. Overall, the modified devices present more robust stability against humidity, thermal stress and light soaking than the control one, following the trend of control<PVK/AS<PVK/AS-BP<PVK/AS-AZO, which corroborates the efficacy of synchronously enhancing the strengthen of chemical and electric field-induced passivation strategies upon constructing robust PSCs.

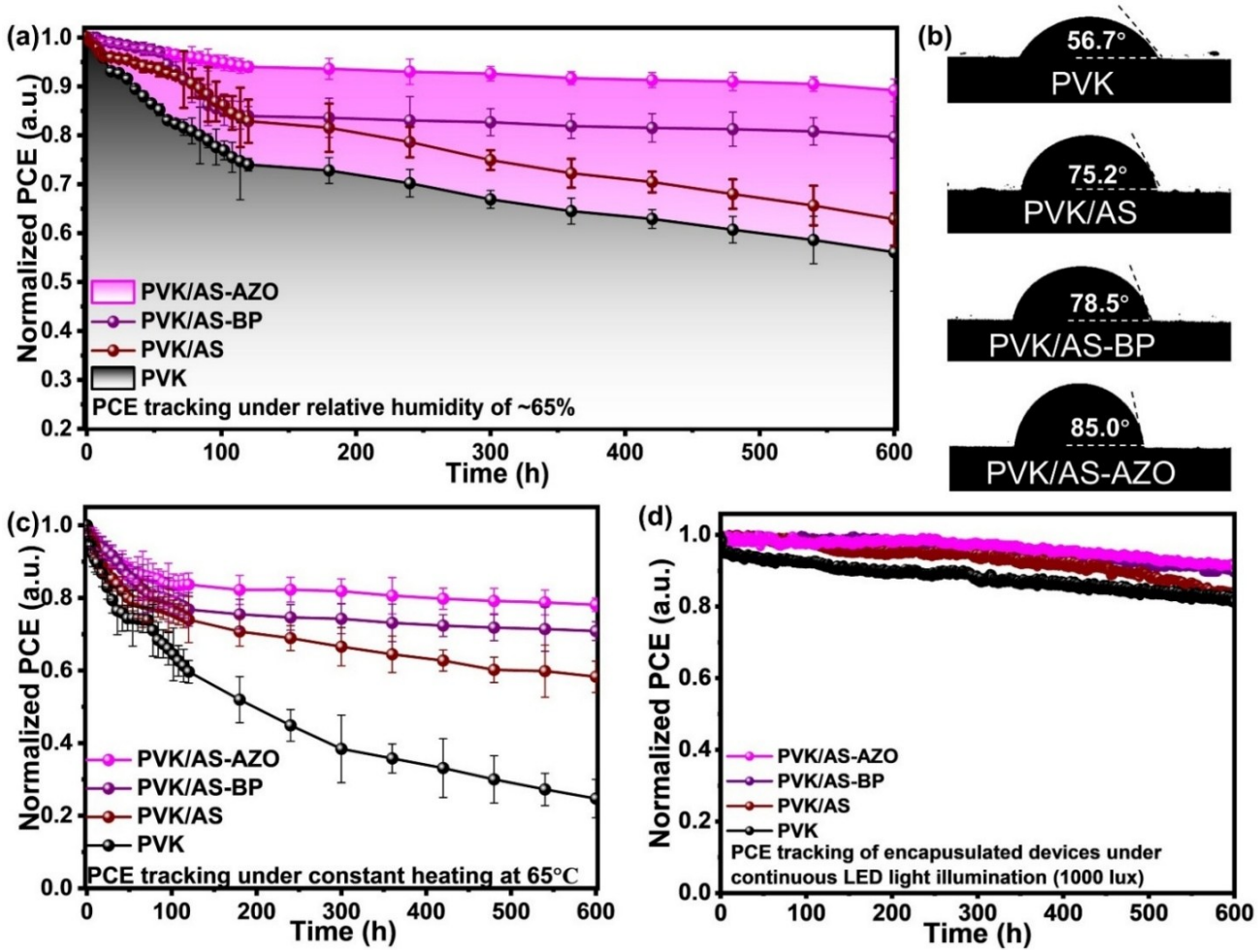

Figure 7. (a) Device stability against high humidity environment with device structure of ITO/SnO2/PVK/Spiro-mF/Au. (b) Water contact angle of perovskite films. (c) Device stability under continuous thermal stress of ~65 °C under a nitrogen atmosphere with device structure of ITO/SnO2/PVK/Spiro-mF/Au. (d) Device stability under continuous LED light illumination under a nitrogen atmosphere with device structure of ITO/SnO2/PVK/Spiro-mF/Au.

3 Conclusions

In summary, we propose an effective passivation strategy that synergistically tunes the chemical and electric filed-induced effects to comprehensively heal the imperfect characteristics of perovskite. The target molecule AS-AZO featuring the most Lewis-base active sites and the largest dipole moment can effectively passivate defects and improve built-in potential. Moreover, the most flexible molecular structure of AS-AZO ensures it as a molecular creeper towards the perovskite grain, not only largely relieving the residual strain, but also reinforcing the overall passivation capability. The overall effects of AS-AZO largely stabilize perovskite and optimize the charge carrier dynamics of derived PSCs, leading to a promising PCE of 25.12% versus that of the control one (21.82%). Besides, the PVK/AS-AZO target devices preserve 93.2% of its initial efficiency after continuous operation for 600 h, implying their superior operational stability.

Acknowledgments: C.T. Qu and H.-L. Loi contributed equally to this work. This work is supported by the National Natural Science Foundation of China (62204079), and the China Postdoctoral Science Foundation (2022M711037). Funding for Key Scientific Research Projects of Higher Education Institutions in Henan Province (25A430027), Postgraduate Cultivating Innovation and Quality Improvement Action Plan of Henan University (SYLYC2022184 and SYLYC2022185). M. Zhang thanks for the financial support from the National Natural Science Foundation of China (62205276), the Hong Kong Research Grants Council (PolyU 15308324), the PolyU Research Center for Organic Electronics (1-CE32) and the PolyU Postdoc Matching Fund Scheme (1-W34A). W.-Y. Wong acknowledges the support from the RGC Senior Research Fellowship Scheme (SRFS2021-5S01), Hong Kong Research Grants Council (PolyU 15307321), Research Institute for Smart Energy (CDAQ), Research Centre for Organic Electronics (CE0P) and Miss Clarea Au for the Endowed Professorship in Energy (847S). F. Yan acknowledges the support from the Research Grants Council Hong Kong (15306822) and Research Center for Organic Electronics of the Hong Kong Polytechnic University (1-CE0P).

Conflict of interest The authors declare that they have no conflict of interest.

Supporting information The supporting information is available online at http://chem.scichina.com and http://link.springer.com/journal/11426. The supporting materials are published as submitted, without typing or editing. The responsibility for scientific accuracy and content remains entirely with the authors

1 Stranks SD, Eperon GE, Grancini G, Menelaou C, Alcocer MJ, Leijtens T, Herz LM, Petrozza A, Snaith HJ. *Science*, 2013, 342: 341-344
2 Zhang Y, Chen Y, Liu G, Wu Y, Guo Z, Fan R, Li K, Liu H, Zhao Y, Kodalle T, Chen Y, Zhu C, Bai Y, Chen Q, Zhou H. *Science*, 2025, 387: 284-290
3 Wu J, Torresi L, Hu M, Reiser P, Zhang J, Rocha-Ortiz JS, Wang L, Xie Z, Zhang K, Park B-w, Barabash A, Zhao Y, Luo J, Wang Y, Lüer L, Deng L-L, Hauch JA, Guldi DM, Pérez-Ojeda ME, Seok SI, Friederich P, Brabec CJ. *Science*, 2024, 386: 1256-1264
4 Zai H, Yang P, Su J, Yin R, Fan R, Wu Y, Zhu X, Ma Y, Zhou T, Zhou W, Zhang Y, Huang Z, Jiang Y, Li N, Bai Y, Zhu C, Huang Z, Chang J, Chen Q, Zhang Y, Zhou H. *Science*, 2025, 387: 186-192
5 Liang Z, Zhang Y, Xu H, Chen W, Liu B, Zhang J, Zhang H, Wang Z, Kang DH, Zeng J, Gao X, Wang Q, Hu H, Zhou H, Cai X, Tian X, Reiss P, Xu B, Kirchartz T, Xiao Z, Dai S, Park NG, Ye J, Pan X. *Nature*, 2023, 624: 7992
6 Park J, Kim J, Yun HS, Paik MJ, Noh E, Mun HJ, Kim MG, Shin TJ, Seok SI. *Nature*, 2023, 616: 724-730
7 Li Q, Liu H, Hou C-H, Yan H, Li S, Chen P, Xu H, Yu W-Y, Zhao Y, Sui Y, Zhong Q, Ji Y, Shyue J-J, Jia S, Yang B, Tang P, Gong Q, Zhao L, Zhu R. *Nat Energy*, 2024, 9: 1506-1516
8 Chen P, Xiao Y, Li S, Jia X, Luo D, Zhang W, Snaith HJ, Gong Q, Zhu R. *Chem Rev*, 2024, 124: 10623-10700
9 Liu H, Gao Y, Xu F, Zhang X, Ullah A, Xu L, Zhang S, Wang J, De Wolf S, Wang HL. *Adv Funct Mater*, 2024, 34: 2315843
10 Yuan L, Zou S, Zhang K, Huang P, Dong Y, Wang J, Fan K, Lam MY, Wu X, Cheng W, Tang R, Chen W, Liu W, Wong KS, Yan K. *Adv Mater*, 2024, 36: 2409261
11 Zhang X, Ding B, Wang Y, Liu Y, Zhang G, Zeng L, Yang L, Li CJ, Yang G, Nazeeruddin MK, Chen B. *Adv Funct Mater*, 2024, 34: 2314529
12 He J, Sheng W, Yang J, Zhong Y, Cai Q, Liu Y, Guo Z, Tan L, Chen Y. *Angew Chem Int Edit*, 2024, 63: e202315233
13 Ma Y, Zeng C, Zeng P, Hu Y, Li F, Zheng Z, Qin M, Lu X, Liu M. *Adv Sci (Weinh)*, 2023, 10: e2205072
14 Xu C, Hang P, Kan C, Guo X, Song X, Xu C, You G, Liao WQ, Zhu H, Wang D, Chen Q, Hong Z, Xiong RG, Yu X, Zuo L, Chen H. *Nat Commun*, 2025, 16: 835
15 Perini CAR, Rojas-Gatjens E, Ravello M, Castro-Mendez AF, Hidalgo J, An Y, Kim S, Lai B, Li R, Silva-Acuña C, Correa-Baena JP. *Adv Mater*, 2022, 34: 2204726
16 Park SM, Wei M, Xu J, Atapattu HR, Eickemeyer FT, Darabi K, Grater L, Yang Y, Liu C, Teale S, Chen B, Chen H, Wang T, Zeng L, Maxwell A, Wang Z, Rao KR, Cai Z, Zakeeruddin SM, Phan JT, Risko CM, Amassian A, Kanatzidis MG, Graham KR, Grätzel M, Sargent EH. *Science*, 2023, 381: 209-215
17 Gao Y, Shen Z, Tan F, Yue G, Liu R, Wang Z, Qu S, Wang Z, Zhang W. *Nano Energy*, 2020, 76: 104964
18 Li D, Li N, Zou C, Zhong Y, Qu Y, Yang S, Wang L, Chen Y, Cheng X, Tao X, Bakr O, Chen Z. *Adv Funct Mater*, 2024, 34: 2313693
19 Duan L, Walter D, Chang N, Bullock J, Kang D, Phang SP, Weber K, White T, Macdonald D, Catchpole K, Shen H. *Nat Rev Mater*, 2023, 8: 261-281
20 Zhu H, Teale S, Lintangpradipto MN, Mahesh S, Chen B, McGehee MD, Sargent EH, Bakr OM. *Nat Rev Mater*, 2023, 8: 569-586
21 Yang J, Sheng W, Li R, Gong L, Li Y, Tan L, Lin Q, Chen Y. *Adv Energy Mater*, 2022, 12: 2103652
22 Zheng Y, Tian C, Wu X, Sun A, Zhuang R, Tang C, Liu Y, Li Z, Ouyang B, Du J, Li Z, Wu X, Chen J, Cai J, Chen CC. *Adv Energy Mater*, 2024, 14: 2304486
23 Qi X, Song C, Zhang W, Shi Y, Gao Y, Liu H, Chen R, Shang L, Tan H, Tan F, Wang HL. *Adv Funct Mater*, 2023, 33: 202214714
24 Hu J, Wang C, Qiu S, Zhao Y, Gu E, Zeng L, Yang Y, Li C, Liu X, Forberich K, Brabec CJ, Nazeeruddin MK, Mai Y, Guo F. *Adv Energy Mater*, 2020, 10: 2000173
25 Yin L, Ding C, Liu C, Zhao C, Zha W, Mitrovic IZ, Lim EG, Han Y, Gao X, Zhang L, Wang H, Li Y, Wilken S, Österbacka R, Lin H, Ma CQ, Zhao C. *Adv Energy Mater*, 2023, 13: 2301161
26 Du S, Huang H, Lan Z, Cui P, Li L, Wang M, Qu S, Yan L, Sun C, Yang Y, Wang X, Li M. *Nat Commun*, 2024, 15: 5223
27 Baumann F, Karimipour M, Padilla-Pantoja J, Chávez-Angel E, Caicedo Roque JM, Pouteaux R, Alcalá Ibarra A, R. Raga S, Santiso J, Lira-Cantu M. *ACS Energy Lett*, 2024, 10: 476-483
28 Tao M, Wang Y, Zhang K, Song Z, Lan Y, Guo H, Guo L, Zhang X, Wei J, Cao D, Song Y. *Joule*, 2024, 8: 3142-3152
29 Dou J, Zhu C, Wang H, Han Y, Ma S, Niu X, Li N, Shi C, Qiu Z, Zhou H, Bai Y, Chen Q. *Adv Mater*, 2021, 33: e2102947
30 Kim SG, Kim JH, Ramming P, Zhong Y, Schotz K, Kwon SJ, Huettner S, Panzer F, Park NG. *Nat Commun*, 2021, 12: 1554
31 Cai S, Gao J, Wu Y, Zou Y, Liang J, Li Y, He X, Cai Q, Wang M, Huang X, Wang X, Sajid S, Wei D, Zhang R, Song D, Wang Y. *Adv Funct*

Mater, 2024, 34: 2411014
32 Che Y, Deng J, Gao Y, Li X, Wang X, Li Y, Zhang J, Yang L. *J Am Chem Soc*, 2024, 146: 26060–26070
33 Meng Y, Wang Y, Liu C, Yan P, Sun K, Wang Y, Tian R, Cao R, Zhu J, Do H, Lu J, Ge Z. *Adv Mater*, 2023, 36: e2309208
34 Wu J, Yan P, Yang D, Guan H, Yang S, Cao X, Liao X, Ding P, Sun H, Ge Z. *Adv Mater*, 2024, 36: e2401537
35 Jeong M, Choi IW, Go EM, Cho Y, Kim M, Lee B, Jeong S, Jo Y, Choi HW, Lee J, Bae J-H, Kwak SK, Kim DS, Yang C. *Science*, 2020, 369: 1615–1620
36 Shah S, Yang F, Köhnen E, Ugur E, Khenkin M, Thiesbrummel J, Li B, Holte L, Berwig S, Scherler F, Forozi P, Diekmann J, Peña-Camargo F, Remec M, Kalasariya N, Aydin E, Lang F, Snaith H, Neher D, De Wolf S, Ulbrich C, Albrecht S, Stolterfoht M. *Adv Energy Mater*, 2024, 14: 2400720
37 Guo Y, Du S, Hu X, Li G, Yu Z, Guan H, Wang S, Jia P, Zhou H, Li C, Ke W, Fang G. *Nano Energy*, 2024, 126: 109612
38 Wang Y, Feng M, Chen H, Ren M, Wang H, Miao Y, Chen Y, Zhao Y. *Adv Mater*, 2024, 36: e2305849
39 Shan T, Zhang Y, Wang Y, Xie Z, Wei Q, Xu J, Zhang M, Wang C, Bao Q, Wang X, Chen CC, Huang J, Chen Q, Liu F, Chen L, Zhong H. *Nat Commun*, 2020, 11: 5585
40 Li X, Weng K, Ryu HS, Guo J, Zhang X, Xia T, Fu H, Wei D, Min J, Zhang Y, Woo HY, Sun Y. *Adv Funct Mater*, 2019, 30: 1906809
41 Lu C, Zhu C, Meng L, Sun C, Lai W, Qin S, Zhang J, Huang W, Du J, Wang Y, Li Y. *Sci China Chem*, 2021, 64: 2035-2044
42 Wang M, Li W, Wang H, Yang K, Hu X, Sun K, Lu S, Zang Z. *Adv Electron Mater*, 2020, 6: 2000604
43 Sun R, Wu Y, Guo J, Wang Y, Qin F, Shen B, Li D, Wang T, Li Y, Zhou Y, Lu G, Li Y, Min J. *Energ Environ Sci*, 2021, 14: 3174-3183
44 Zhang S, Bi F, Han J, Shang C, Kang X, Bao X. *Nano Energy*, 2022, 102: 107742
45 Du T, Qiu S, Zhou X, Le Corre VM, Wu M, Dong L, Peng Z, Zhao Y, Jang D, Spiecker E, Brabec CJ, Egelhaaf H-J. *Joule*, 2023, 7: 1-18
46 Duan X, Liu C, Cai Y, Ye L, Xue J, Yang Y, Ma W, Sun Y. *Adv Mater*, 2023, 35: e2302927
47 Xiang J, Han C, Qi J, Cheng Y, Chen K, Ma Y, Xie J, Hu Y, Mei A, Zhou Y, Han H. *Adv Funct Mater*, 2023, 33:
48 Gao Y, Xiao Z, Cui M, Saidaminov MI, Tan F, Shang L, Li W, Qin C, Ding L. *Adv Mater*, 2024, 36: 2306373
49 Gao W, Liu T, Sun R, Zhang G, Xiao Y, Ma R, Zhong C, Lu X, Min J, Yan H, Yang C. *Adv Sci (Weinh)*, 2020, 7: 1902657
50 Wang Y, Gu S, Liu G, Zhang L, Liu Z, Lin R, Xiao K, Luo X, Shi J, Du J, Meng F, Li L, Liu Z, Tan H. *Sci China Chem*, 2021, 64: 2025-2034
51 Feng K, Huang J, Zhang X, Wu Z, Shi S, Thomsen L, Tian Y, Woo HY, McNeill CR, Guo X. *Adv Mater*, 2020, 32: 2001476
52 Liu T, Ma R, Luo Z, Guo Y, Zhang G, Xiao Y, Yang T, Chen Y, Li G, Yi Y, Lu X, Yan H, Tang B. *Energ Environ Sci*, 2020, 13: 2115-2123
53 Peng Y, Chen Y, Zhou J, Luo C, Tang W, Duan Y, Wu Y, Peng Q. *Nat Commun*, 2025, 16: 1252
54 Li Z, Wu M, Yang L, Guo K, Duan Y, Li Y, He K, Xing Y, Zhang Z, Zhou H, Xu D, Wang J, Zou H, Li D, Liu Z. *Adv Funct Mater*, 2023, 33: 2212606
55 Xiang J, Cheng Y, Zhang G, Liu Z, Han C, Gao Q, Wang C, Xie J, Li S, Zhou Z, Liu J, Lu X, Mei A, Zhou Y, Han H. *Adv Funct Mater*, 2024, 34:
56 Xiang J, Han C, Cheng Y, Gao Q, Hu W, Zhou Y, Mei A, Zhou Y, Han H. *Adv Mater*, 2025, 37:
57 Ji X, Feng K, Ma S, Wang J, Liao Q, Wang Z, Li B, Huang J, Sun H, Wang K, Guo X. *ACS Nano*, 2022, 16: 11902-11911
58 Feng X, Gao Y, Huang X, Wang J, Dong C, Yue G, Tan F, De Wolf S. *Small*, 2024, 20: 2403267
59 Yan K, Shen Z, Niu B, Huang Y, Wang D, Gu E, Yan B, Yao J, Chen H, Li C-Z. *Sci China Chem*, 2023, 66: 1795-1803
60 Peplow M. *Nature*, 2023, 623: 902-905
61 Shen L, Song P, Jiang K, Zheng L, Qiu J, Li F, Huang Y, Yang J, Tian C, Jen AK, Xie L, Wei Z. *Nat Commun*, 2024, 15: 10908
62 Wang ZS, An Y, Ren X, Zhang H, Huang Z, Yip HL, Huang Z, Choy WCH. *Nat Commun*, 2024, 15: 9647
63 Yang Y, Xiong Q, Wu J, Tu Y, Sun T, Li G, Liu X, Wang X, Du Y, Deng C, Tan L, Wei Y, Lin Y, Huang Y, Huang M, Sun W, Fan L, Xie Y, Lin J, Lan Z, Stacchinii V, Musiienko A, Hu Q, Gao P, Abate A, Nazeeruddin MK. *Adv Mater*, 2024, 36: 2310800
64 Chen S, Hong L, Dong M, Deng W, Shao L, Bai Y, Zhang K, Liu C, Wu H, Huang F. *Angew Chem Int Edit*, 2023, 62: e202213869

Table of Contents

A synchronous modulation strategy of the chemical and electric field-induced passivation effects was proposed to comprehensively heal imperfect characteristics of perovskite. The target molecule AS-AZO featuring the most Lewis-base active sites and the largest dipole moment effectively passivate defects of perovskite and improve built-in potential of PSCs. Moreover, the most flexible structure of AS-AZO ensures it as a molecular creeper towards perovskite grain, not only relieving residual strain, but also reinforcing the overall passivation capability. The overall effects of AS-AZO largely stabilize perovskite and optimize the charge carrier dynamics of PSCs, resulting in a promising PCE of 25.12% and robust stability.